



PAYLOAD CALIBRATION

Calibration of Scanning Sky Monitor (SSM) onboard AstroSat

ABHILASH R. SARWADE^{1,*}, M. C. RAMADEVI¹, B. T. RAVISHANKAR¹,
BRAJPAL SINGH¹, BLESSY ELIZABETH BABY¹, DIPANKAR BHATTACHARYA²
and S. SEETHA³

¹Space Astronomy Group, ISITE Campus, U.R. Rao Satellite Centre, Outer Ring Road, Marathahalli, Bengaluru 560 037, India.

²Inter-University Centre for Astronomy and Astrophysics, Ganeshkhind, Pune 411 007, India.

³Department of Astronomy and Astrophysics, Raman Research Institute, Sadashivanagar, Bengaluru 560 080, India.

*Corresponding Author. E-mail: sarwade@urisc.gov.in

MS received 7 November 2020; accepted 22 April 2021

Abstract. SSM onboard AstroSat is designed to monitor X-ray sky in the energy range 2.5–10 keV to detect and locate X-ray sources in outburst. SSM with its three almost identical 1D-proportional counters mounted on a rotating platform, scans the sky in step and stare mode of operation. It observes the X-ray sky and generates light curves for X-ray sources detected. Here, we discuss the positional calibration to carry out imaging with SSM. Onboard calibration of SSM has been carried out with Crab, the standard X-ray source. SSM observations of Crab are compared with that of MAXI on ISS for cross calibration of the instrument.

Keywords. Proportional counter—position sensitive X-ray detector—sky monitor—X-ray sky—coded-mask—X-ray transient.

1. Introduction

Scanning Sky Monitor (SSM) is a wide field soft X-ray imaging payload on AstroSat. SSM is one of the five payloads onboard AstroSat (Agrawal 2006; Singh & Tandon 2014; Agrawal 2017). SSM with its large Field of View (FoV) scans the X-ray sky continuously in step and stare mode of operation to detect and locate transient X-ray sources. The primary objective of SSM is to monitor the X-ray sky for transient activity in the X-ray in the energy range 2.5–10 keV, both in known sources and new ones.

SSM consists of three coded mask cameras, mounted on a rotating platform, so as to enable near complete coverage of the sky. The platform rotates in step and stare mode from 5° to 355° and back. Every stare is for a duration of 10 minutes, by default. After

each stare, the platform steps by 10° to change the FoV of the SSM cameras. The mounting of the three units of SSM cameras is shown in figure 1. The entire assembly rotates about the +Yaw axis of the spacecraft. A detailed description of the instrument can be found in Seetha *et al.* (2006) and Ramadevi *et al.* (2017).

2. Imaging with SSM

The coded-mask along with the position-sensitive anodes in the detectors in SSM acts as the imaging element in the instrument. When X-rays enter through the coded mask plate which contains random pattern of slits, shadows of the mask are cast on the position-sensitive anode wires. The position and intensity of these shadows are a function of the incidence angle of the incoming X-rays relative to the mask-detector axis. This information is used in deriving the position of the X-ray source. The position of interaction of the incident X-ray photon in a position sensitive anode

This article is part of the Special Issue on “AstroSat: Five Years in Orbit”.

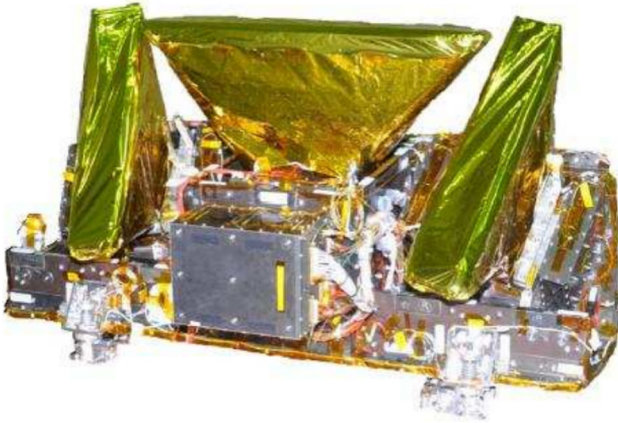


Figure 1. SSM instrument with three cameras mounted on a platform.

wire in the proportional counter is inferred from the ratio of the charge output measured on both ends of a resistive anode wire. The charge ratio of every photon incident on the detector plane is used to obtain the position of incidence on the anode wire in the detector plane. The detector plane comprises eight anodes in each SSM camera. The position of incidence of all the photons is binned in order to get the position histogram on the detector plane which is defined as the Detector Plane Histogram (DPH). The DPH is in principle the shadow of the mask pattern which is illuminated for a particular angle of incidence of the X-ray source in the FoV. In order to derive the position of every photon incident on the detector plane it is required to obtain the relation between the charge ratio and the geometric position along the anode wire in the detector.

3. Position calibration

In order to carry out imaging with SSM, the detectors are calibrated for positional response. Position calibration is undertaken to determine the relation between the charge ratio of the photon event incident and the position of its interaction in the detector plane, which is called the calibration function. Each anode is independent from the other and there are eight anodes in each SSM unit for which this calibration has to be done. Positional calibration of SSM detectors involves derivation of the calibration function for each of the eight anode wires in all three SSM units. Imaging is carried out using the shadow generated by binning the position of incident events to get the DPH. Details of ground calibration of SSM can be found in Ramadevi *et al.* (2011). Onboard calibration involves observing

Crab, the standard X-ray source, with SSM at different locations in its FoV.

4. Mathematical model of calibration function

Figure 2 describes schematic diagram of a single anode wire. The length of the anode wire that is exposed to incident X-rays is 60 mm. However, the electrical length of the anode wires may not be 60 mm. This is because the anode wires are glued, using conductive silver epoxy, to conductive high voltage grooves placed inside the insulator (Kelvin-F) which is fixed into the wire-module of the detector. The glue is applied from one end of the groove, and the position where the wire makes electrical contact may be at the inner edge of the groove (at the geometric end point of wire) or anywhere within the length of the groove. Due to this reason, the start and end points of the resistive anode wire which defines the length, varies from wire to wire. Thus, it is not possible to get the length of the anode wires from mechanical dimensions of the detector. Therefore, it is necessary to know the electrical length of the anode wires (which is the length seen by the charge cloud) to derive the position of photons incident on the detector.

We define $x = 0$ as the mid-point (geometric mid point) of the exposed anode wire as shown in Fig. 2 and $x = l_L$ and $x = -l_R$ as left end and right end of anode wire respectively, which extend till the conductive point inside the Kel-F grooves on either ends of the wire, in the wire module. Note that l_L and l_R are not necessarily same. There is a calibration wire of diameter 2 mm which is placed above the window of the detector across the anode wires at the geometric centre of the anode wires so that this casts a shadow on the anode wire for incident X-rays, which is used as a reference for geometric centre of the anode wires in the detector plane.

When a X-ray photon is photoelectrically absorbed, a charge cloud is created due to the movement of the electrons towards the high voltage applied on the anode wire. The charge cloud is detected on the anode wire at position, say $x = x_0$ on the anode wire, the total collected charge Q is divided on left and right as

$$Q_L = Q \times \frac{l_R + x_0}{l_L + l_R},$$

$$Q_R = Q \times \frac{l_L - x_0}{l_L + l_R}.$$

As shown in Fig. 2, ends of anode wire are connected to Charge Sensitive Pre-Amplifiers (CSPAs) followed

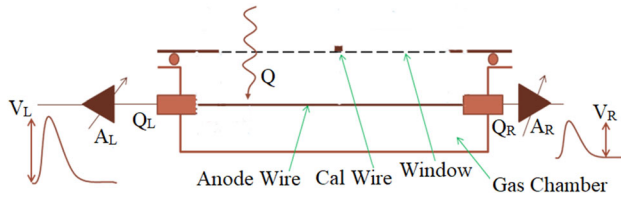


Figure 2. Schematic diagram of an anode wire.

by post-amplifiers with a finite gain given by amplification factors A_L and A_R . Therefore, the signals detected at the ends of anode wire are given by

$$V_L = A_L \times Q_L = A_L \times Q \times \frac{l_R + x_0}{l_L + l_R},$$

$$V_R = A_R \times Q_R = A_R \times Q \times \frac{l_L - x_0}{l_L + l_R}.$$

The voltage ratio $R = \frac{V_L - V_R}{V_L + V_R}$ can be used as indicative of the position of the X-ray interaction. Simplifying, ratio can be expressed as

$$R = \frac{A_L(l_R + x_0) - A_R(l_L - x_0)}{A_L(l_R + x_0) + A_R(l_L - x_0)}.$$

Inverting the above equation to express position of interaction of X-ray photon in terms of ratio, we get

$$x_0 = \frac{R(A_R l_L + A_L l_R) + (A_R l_L - A_L l_R)}{R(A_R - A_L) + (A_R + A_L)}.$$

This is calibration function with l_L , l_R and A_L , A_R as unknown calibration constants for each anode wire.

5. Estimation of calibration constants

5.1 Calibration data

Onboard calibration of SSM cameras are carried out by observing Crab, the standard X-ray source. In order to estimate the calibration constants, SSM camera was pointed towards Crab with the X-ray source positioned at about the center of camera's FoV (location of Crab in the FoV of SSM: $(\theta_x, \theta_y) = (0.62^\circ, 0.52^\circ)$). The source, Crab was chosen due to its relatively stable intensity in the SSM's energy range and sufficiently good count rate along with its position in relatively clean portion of the X-ray sky with no other bright sources nearby. The calibration data was acquired for an exposure time of about 15 ks. The data was filtered based on following conditions to generate Good Time Intervals (GTIs):

- Crab not occulted by Earth

- Satellite not in SAA
- Earth not in the FoV
- Energy between 2.5 keV to 10 keV
- Lower particle background (see Section 7)
- Absence of any attitude variation

Figure 3 shows the data selection according to the GTI generated with the above mentioned conditions for one orbit. Similarly data is filtered for all the orbits as per the GTIs. The effective exposure time, after GTI filtration, is about 10 ks. This data is used to generate the observed DPH for a given source location.

5.2 Monte Carlo simulations

For a given source location in the FoV, it is required to simulate the expected DPH for calibrating it with the observed DPH. In order to simulate the shadows registered by the SSM cameras, Monte Carlo methods are employed. All the measured geometric parameters of the cameras are considered to make their model. Among the three SSM cameras, the two edge cameras are physically identical and the central camera has different dimensions. The physical dimensions considered in the model include: (a) the mask plate dimensions including inter-pattern gaps, plate thickness, and the six different patterns, (b) the detector module with individual anode placements in respective wire-cells, (c) the window and the window support rods, (d) calibration wire, and so on. The six mask plates considered for the cameras, joined sideways, each consist of 63 mask elements of open and closed elements which are represented in the model respectively as 1's and 0's. In order to simulate the photon strike over the mask plate, random number generation has been employed based on Park Miller Minimal standard algorithm with shuffling (Press *et al.* 1992). If the random position on the mask plate falls in an open element, for the given incidence angles, θ_x and θ_y , it is checked which wire cell it can strike. This is registered only if the photon's trajectory does not hit any of the structural elements of the camera, either in the mask plate (such as, within the plate thickness or the ribs), window support rods or the calibration wire. For incidences away from the normal, slant-ray effects affecting the photon trajectory are also considered along both x and y directions. Also considered are the quantum efficiency effects which in turn depend on energy-band specific mean-free path value and

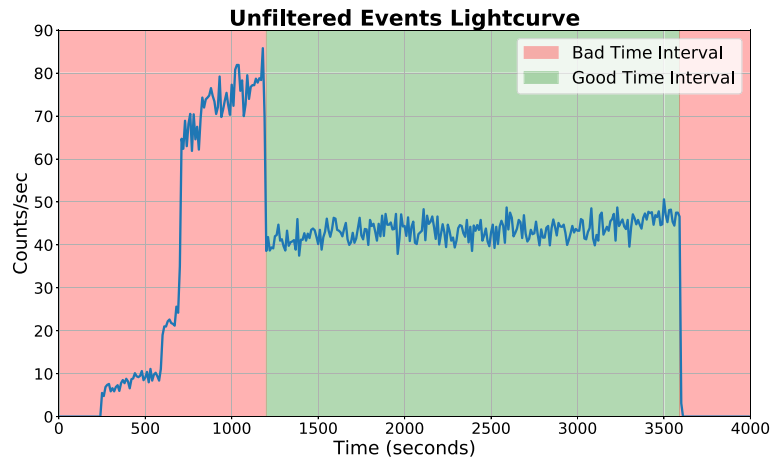


Figure 3. Good Time Interval (GTI) selection.

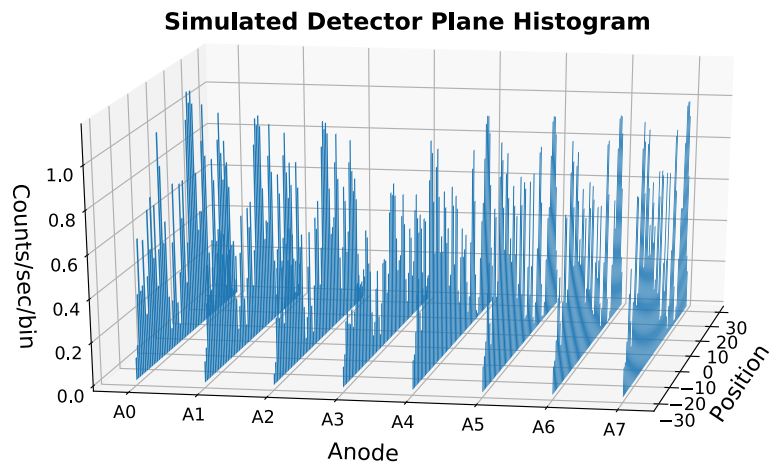


Figure 4. Simulated Detector Plane Histogram (DPH) with each anode wire of 60 mm length divided into 63 bins along the anode wire.

attenuation due to the aluminised Mylar window. After applying all these corrections on the histogram of the detector strike positions of the events, the uncertainty in reading out is simulated by introducing a Gaussian smear of position resolution σ varying along the length of the anode wires by $\sim 0.5\text{--}1.2$ mm. The DPH (see Fig. 4) thus generated is used for further modelling. For the better visualization of DPH, each anode's histogram is plotted side by side (see Fig. 5). The simulated DPH for anode A0 is shown in Fig. 6 for better visualization of shadows incident on anode wires.

5.3 Derivation of calibration constants

The observed data is used to generate the ratio histogram of the charge ratios of all the events incident on the respective anode wires. This gives the shadow pattern in ratio domain and the simulated

DPH gives the shadow pattern in position domain. For a given source location, the two patterns are matched to get the ratio to position map for all the eight anode wires. The maximas and minimas of observed ratio DPH are matched with respective maximas and minimas of the simulated position DPH as shown in Fig. 7. This process is carried out independently for each anode wire of all SSM cameras. For the purpose of illustration, we demonstrate the calibration process for one of the anodes, A0 of SSM1. The same procedure is followed for all other anodes in SSM. The simulated DPH for anode A0 is shown in Fig. 6. The calibration constants l_L , l_R and A_L , A_R for every anode is derived by obtaining the calibration function using the ratio and position values.

Therefore, given the pairs of ratio and position, the calibration equation is fit to estimate the calibration constants. These calibration constants are used to convert the charge ratio of every incident photon on

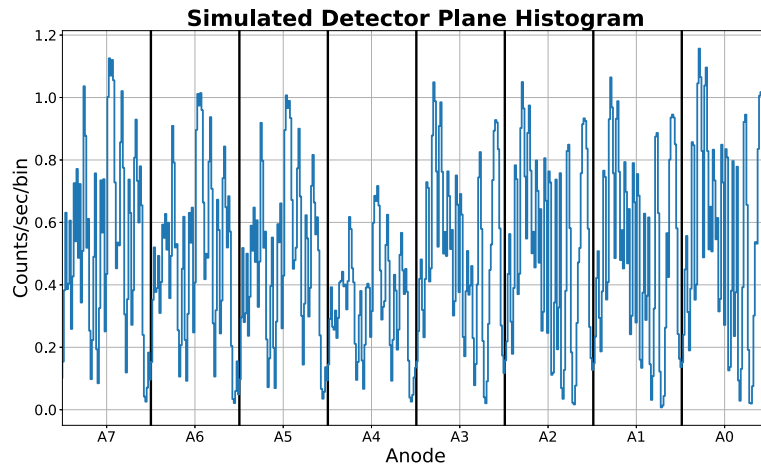


Figure 5. Simulated Detector Plane Histogram (DPH) of all eight anode wires (named A0 to A7) with each anode's histogram plotted side by side for better visualization.

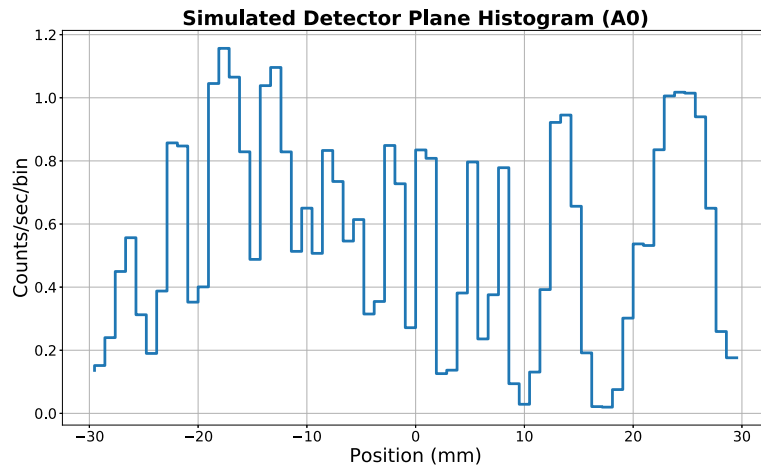


Figure 6. Simulated Detector Plane Histogram (DPH) for anode A0.

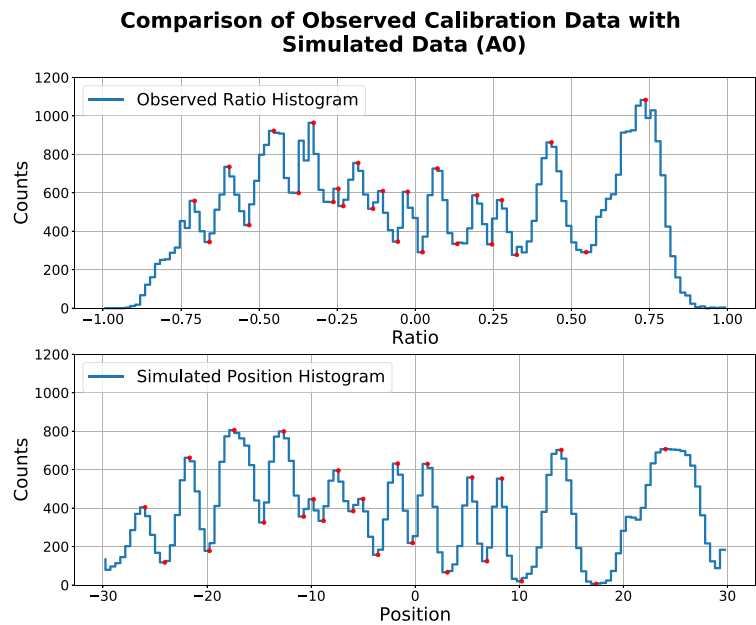


Figure 7. Comparison of observed calibration data with simulated data (A0).

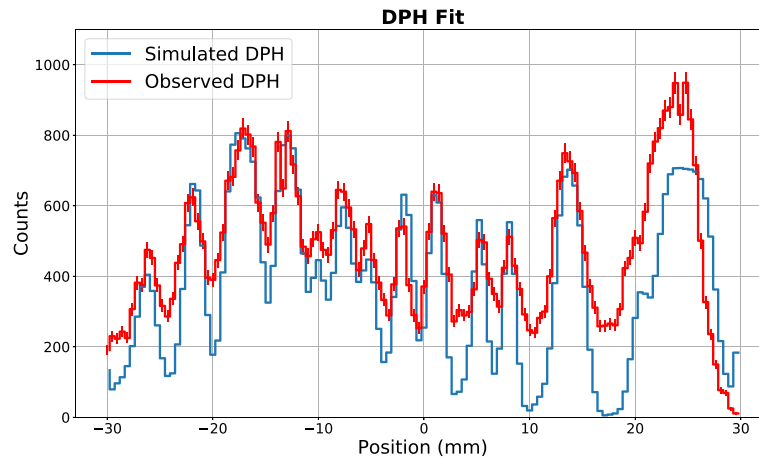


Figure 8. Comparison between simulated DPH and observed DPH. The observed DPH is obtained using the estimated calibration constants.

the detector plane to position. Position of the events in the respective anodes are binned to get the observed DPH which is then compared with that of the simulated DPH as shown in Fig. 8.

6. Anode response

Anodes in SSM are position sensitive resistive wires and the relative detection efficiency from one position bin to the other along the anode wire are not the same. This non-uniform variation along the anode wire is called the anode response and is one of the aspects of the calibration database for imaging with SSM. The observed DPH has the anode response already included, as it is part of the instrument response and this has to be appropriately handled while fitting the observed with the simulated DPH in imaging. The anode response is estimated with uniform illumination of the source along the anode wires for all SSM cameras during ground calibration.

6.1 Anode response from ground calibration

Each SSM unit is illuminated with an X-ray source so that the detector plane with eight anodes is uniformly illuminated. The anode responses are derived from this after removal of the source illumination profile as the X-ray source used is a diverging source. The non-uniform anode response along the anode wires are modelled using the ground calibration data with uniform illumination of SSM detectors. The DPH modelled as anode response as shown in Fig. 9.

7. Background modelling

The detector background in SSM has two components: X-ray sky background and charged particles. The veto layer inside the SSM detector module is an additional layer of anode wire beneath the main anode wires. This layer is meant to reject charged particles that are incident via the anti-coincidence technique.

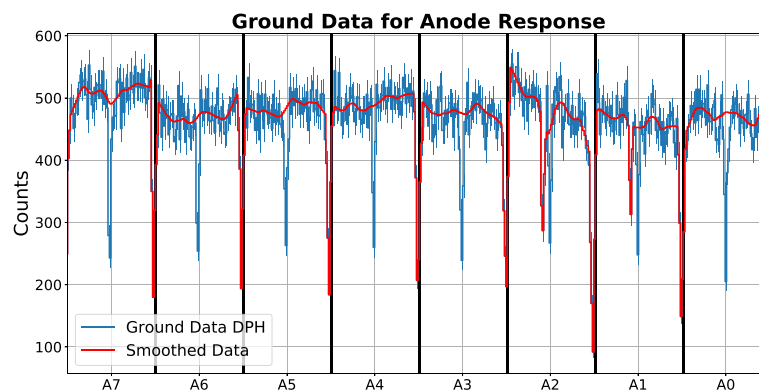


Figure 9. Ground Data DPH used to derive anode response.

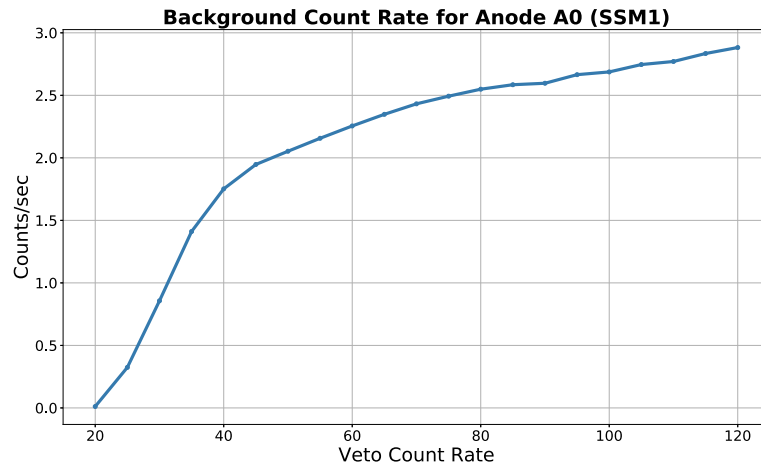


Figure 10. Background count rate as a function of veto count rate for anode A0 of SSM1.

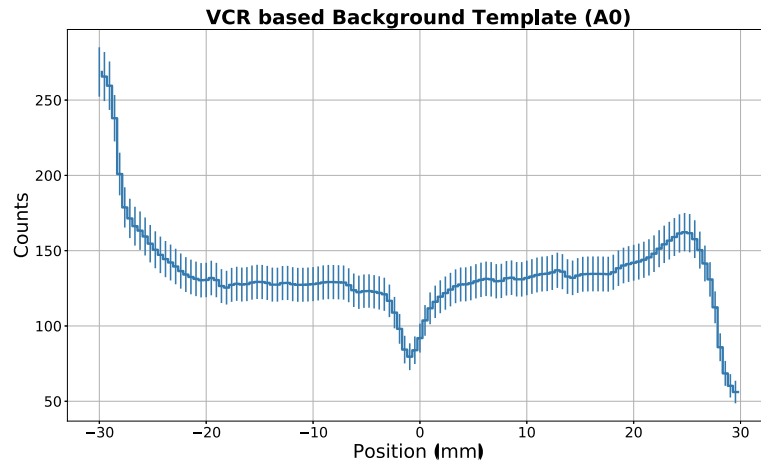


Figure 11. Background template generated based on observed VCR during calibration observation for anode A0.

The rate of events detected in this layer (called the Veto Count Rate (VCR)) are largely counted as charged-particle background. During the ingress and egress of SAA region, the contribution from charged particles is rather high which is indicated by increase in VCR in SSM. The charged particle counts detected in SSM is modelled with veto count rates detected in every stare.

While estimating calibration constants from the Crab calibration data, the X-ray and particle background contribution must also to be taken into account. In order to model the background contribution in the DPH, data from faint field observations were aggregated. A faint field is regarded as one in which the total flux incident on the camera is less than $0.5 \text{ photons/cm}^2/\text{s}$ so that, it can be considered that all the events registered during these faint field observations are due to background. The background count rate in the field of view is related to that of the veto count rate as shown in Fig. 10.

Background templates are generated using the VCR for every stare and used in the estimation of calibration constants as discussed in this paper. These background templates generated are also being used for imaging. Background template for the calibration data is shown in Fig. 11.

Both the anode response and the background model are used to generate the observed DPH and compared with that of the simulated DPH as shown in Fig. 12.

8. Conclusion

Different aspects of position calibration of SSM are discussed in the previous sections. The calibration database is generated for all three SSM cameras and are used in imaging with SSM. Calibration observations of Crab with SSM have been extensively studied with respect to various aspects of image processing. The calibration database obtained as per the procedure

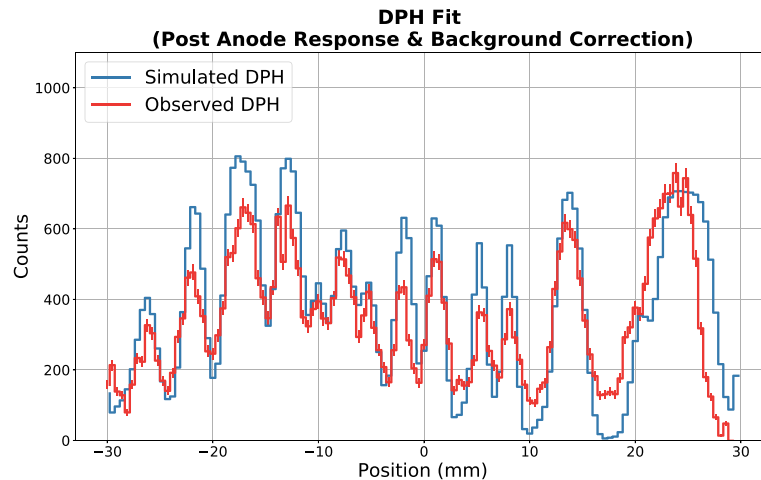


Figure 12. Comparison between simulated DPH and observed DPH. The observed DPH is obtained using estimated calibration constants, multiplying with anode response and subtracting background model.

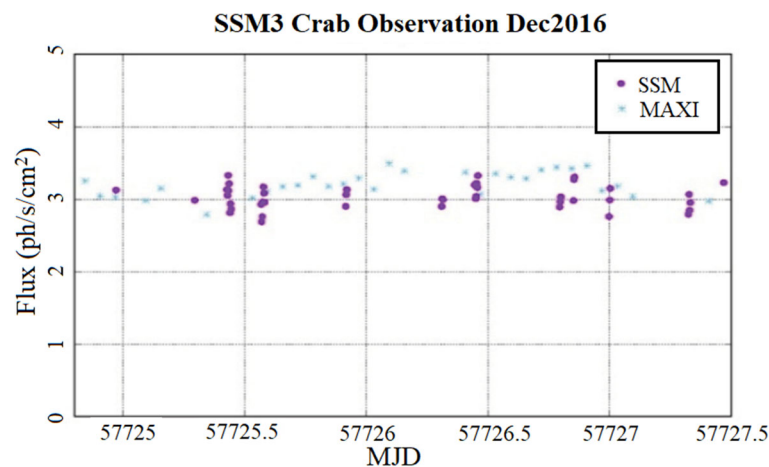


Figure 13. Crab light curve compared with that of MAXI.

discussed here, along with the background modelling, are applied to the data to get the Crab flux consistent to a level of $\pm 15\%$ as shown in Fig. 13. The results are compared with that of MAXI onboard ISS as part of cross calibration and are found consistent.

SSM data for all other sources observed till date are being reprocessed and the database of the light-curve for these sources will be updated in the SSM website hosted at ISSDC. A more detailed investigation is in progress and the results will be reported in due course.

Acknowledgements

The authors acknowledge Director, URSC and DD, PDMSA and GH, SAG for the constant support and also acknowledge various entities at ISRO who have

contributed their part towards realization of all aspects of the instrument.

References

- Agrawal P. C. 2006, Adv. Space Res., 38(12), 2989
- Agrawal P. C. 2017, J. Astrophys. Astr., 38, 27
- Press W. H., Teukolsky S. A., Vetterling W. T., Flannery B. P. 1992, Numerical Recipes in C: The Art of Scientific Computing, 2nd edition, Cambridge University Press.
- Ramadevi M. C., Ravishankar B. T., Seetha S. 2011, Exp. Astron., 31(2–3), 99
- Ramadevi M. C., Seetha S., Bhattacharya D. *et al.* 2017, Exp. Astron., <https://doi.org/10.1007/s10686-017-9536-3>
- Seetha S., Ramadevi M. C., Babu V. C. *et al.* 2006, Adv. Space Res., 38, 2995
- Singh K. P., Tandon S. N. *et al.* 2014, Proc. of SPIE, 91442T, 9144-100-100, <https://doi.org/10.1117/12.2062667>